TEST Engineering & Management

May – June 2020
ISSN: 0193-4120 Page No. 1163 - 1167

Burr Control using Modified Tool Geometry: A 3D FEM Approach

Muhammad Asad

Article Info
Volume 83
Page Number: 1163 - 1167
Publication Issue:
May - June 2020

Article History
***Article Received**: 11August 2019*
***Revised**: 18November 2019*
***Accepted**: 23January 2020*
***Publication**:10 May2020*

Abstract:

This work presents finite element based 3D-machining simulations. Cutting simulations for orthogonal machining case for AA2024-T351 are performed. Quantitative predictions of negative burr lengths on machined workpiece-end, alongwith specific chip shape formation has been made. Numerically acquired chip geometrical shape and results of machining forces are compared with the associated experimental results from literature. Onwards, machining simulations with a modified cutting tool geometry have been reproduced. It has been found that convex shape modified tool geometry helps to restrict early formation of crack in front of tool and control the material deformation in cutting direction. This helps reducing material flow towards edges and formation of exit burr and edge breakout.

***Keywords:** Machining simulation, chip formation, negative burr, burr control*

I. INTRODUCTION

Machining is widely used manufacturing process to acquire high surface finish and precise work parts. In all sort of machining process like turning, milling, broaching, drilling, sawing, etc. sharp and non-value added material is produced on workpiece edges, normally called as “burr”. Burr must be removed prior to the next function of the machined component; either to be used in assembly or for any further processing like heat treatment, surface plating, etc. Depending on materials, dimensions, and quality of the final product various deburring methods are employed in industry [1-2]. These post machining deburring processes eventually increase cost of final products and effect their timely delivery to assembly lines. Numerous researches have been made to comprehend and control burr formation during cutting processes. These include studies on various types of burr formation mechanisms [2], tool geometry selection [3], and range of cutting parameters [4], tool path planning [5] and workpiece geometry design [6]. In this continuation, present work proposes a modified turning insert geometry to reduce the negative burr formation and edge breakout at the tool exit. The work exploits the FE based cutting model established for machining of aluminum alloy AA2024-T351 [7]. Initially, orthogonal turning simulations for cutting speed = 800 m/min, feed = 0.4 mm/rev, depth of cut = 4 mm with an insert profile of commercially available tool (Sandvik insert: CCGX 12 04 08-AL H10) have been produced. Numerical results concerning chip geometrical shape and machining forces (in cutting direction along x-axis) are matched with related experimental results from literature [7]. Negative burr formation and edge breakout with various process parameters are quantified. Onwards, new proposed tool has been used to rerun the cutting simulations. Promising results in reducing negative burr at exit edge have been found with convex shaped modified tool geometry.

II. MATERIAL CONSTITUTIVE MODEL, TOOL AND WORKPIECE GEOMETRY AND HYPOTHESIS

The realized geometrical model for orthogonal cutting case is shown in Fig.1. Tool geometry and cutting angles are same as that used in experimental work. Whereas, a curvature radius of 12mm (equals to width of actual insert used in experimental work [7]) has been made to the tool rake face to run cutting simulation with modified tool geometry, as depicted in Fig. 1. During simulation tool can advance in cutting direction (negative x-axis direction). While for workpiece lower plane, the degree of freedom is fully constrained. To realize chip separation ductile fracture approach is adopted in the work [8-9]. A chip separation area is modelled in this context. Thickness of this area is kept 20μm (equals cutting edge radius [10-11]). While predefined chip section represents feed and depth of cut (DOC), while below the chip separation area is the machined work part. All these three parts of workpiece are assembled using Abaqus

May – June 2020
ISSN: 0193-4120 Page No. 1163 - 1167

inbuilt tie constraint algorithm, so that during simulation, they behave as single entity. During machining, heat produced due to friction and plastic work therefore, thermally coupled C3D8RT elements have been used to mesh tool and workpiece parts.

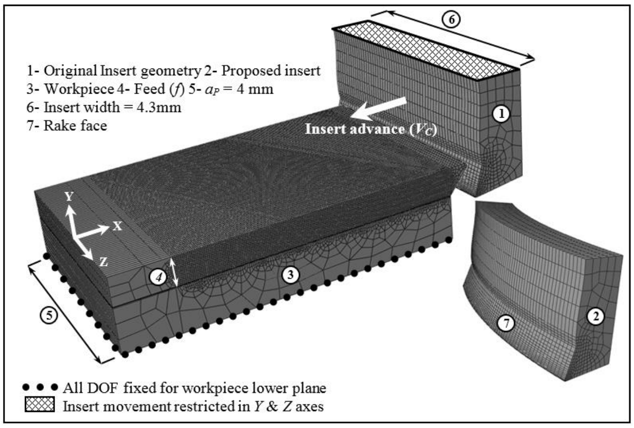

Fig.1 Orthogonal cutting model

Classical Coulomb`s friction is employed to characterize friction at tool and work interaction level. Flow stresses are based on Johnson-cook constitutive model (equation (1)). Furthermore, to simulate ductile damage, Johnson-cook damage model equation (2)) is used.

$$\bar{\sigma}_{JC} = \underbrace{\left(A+B\bar{\varepsilon}^{n}\right)}_{\text{Elasto-plastic term}} \underbrace{\left[1+C\ln\left(\frac{\dot{\bar{\varepsilon}}}{\dot{\bar{\varepsilon}}_0}\right)\right]}_{\text{Viscosity term}} \underbrace{\left[1-\left(\frac{T-T_r}{T_m-T_r}\right)^{m}\right]}_{\text{Softening term}} \quad (1)$$

$$\bar{\varepsilon}_{0i} = \left[D_1 + D_2 exp\left(D_3 \frac{P}{\bar{\sigma}}\right)\right] \times \left[1+D_4 ln\left(\frac{\dot{\bar{\varepsilon}}}{\dot{\bar{\varepsilon}}_0}\right)\right] \left[1+D_5\left(\frac{T-T_r}{T_m-T_r}\right)\right] \quad (2)$$

Equation (2) is used to calculate scalar damage initiation parameter ω (equation (3)). Damage in a specific mesh element is initiated once "ω" approaches numeric value of one.

$$\omega = \sum \frac{\Delta\bar{\varepsilon}}{\bar{\varepsilon}_{0i}}$$

(3)

Hillerborg [12] energy approach is used to model fracture.

$$G_f = \int_0^{\bar{u}_f} \sigma_y d\bar{u}$$

(4)

The failure displacement, $\bar{u}_f$ is calculated by following relation:

$$\bar{u}_f = \frac{2G_f}{\sigma_Y}$$

(5)

Provided material fracture toughness, K_C the fracture energy, G_f is calculated by equation (6)

$$\left(G_f\right)_{I,II} = \left(\frac{1-\nu^2}{E}\right)\left(K_C^2\right)_{I,II}$$

(6)

Damage (D) in a material element evolves linearly (equation (7)) or exponentially (equation (8))

$$D = \frac{\bar{u}}{\bar{u}_f}$$

(7)

$$D = 1-\exp\left(-\int_0^{\bar{u}} \frac{\bar{\sigma}}{G_f} d\bar{u}\right)$$

(8)

Table 1. Materials properties [7]

Parameters	Work AA2024	Tool (Tungsten carbide`
Density, ρ	2700	11900
Young`s modulus, E	73000	534000
Poisson`s ratio, ν	0.33	0.22
Fracture energy, G_f	20E3	Nil
Specific heat, C_p	0.557T+877.6	400
Expansion coeff., α_d	8.9^{-3}T+22.2	Nil
Thermal conductivit	25 ≤T≤ 300: λ=0.247T+114.4 300 ≤T≤ T_m: λ=-0.125T+226	50
Meting temperature	520	Nil
Room temperature	25	25
Fracture toughness (K_{IC} and K_{IIC})	26 and 37	Nil

Element`s stiffness fully degrades as damage parameter (D) acquires value equals one, onwards relevant element is deleted. Thus, chip separation from work body is realized. Table 1and Table 2 provide tool and work properties.

Table 2. Damage model parameters [7]

A	B	n	C	m	D_1	D_2	D_3	D_4	D_5
352	440	0.4	0.0083	1	0.13	0.13	-1.5	0.01	0

III. Results and Discussions

Orthogonal cutting simulation for Cutting speed (V_C) = 800 m/min, feed (f) = 0.4 mm/rev, depth of cut *(DOC)* = 4 mm with an insert profile of commercially available turning insert (original insert) and new modified tool (MT) geometry are performed and various results concerning, chip evolution, cutting forces and negative burr formation are discussed in the section.

TEST Engineering & Management

May – June 2020
ISSN: 0193-4120 Page No. 1163 - 1167

Negative burr formation with original insert

Figure 2a, represents 3D continuous chip morphology which is in good correlation with the experimental chip (Fig. 2b). While numerically calculated cutting force of 901N is also in a close match with experimentally registered force of 974 N [7]. During cutting as tool approaches the end of workpiece it applies bending load on exit end of workpiece (Figure 3a). As tool further advances towards workpiece end the bending load on workpiece edge keeps on increasing. This promotes large plastic deformation initiation from workpiece end. This plastic deformation initiation point; which can be seen below machined workpiece surface, is termed as pivot point [2]. The large deformation zone around pivot point termed as "negative shear zone" keeps on enlarging and ultimately connects with primary shear zone. Formation of pivot point and generation of negative shear zone at the middle section (Z = 0) along depth of cut is shown in Fig.3a and 3b. As tool keeps on advancing towards workpiece end, material escapes from actual cutting action. Material separates from workpiece by crack formation that initiates from tool nose and leads to the workpiece end. Finally, a boot type chip is formed (Fig. 4a). Boot chip also takes away some material from the edge of the machined workpiece termed as edge breakout or negative burr. The final machined workpiece edge geometry is broken and deformed. Fig. 4a, quantifies the broken workpiece edge geometry (negative burr) along x and y-axes. Similar dimensions of the boot chip and negative burr can be figured out at other sections along depth of cut, like Z = ±1.5 and ±2 in Fig. 5a and 5b, respectively.

Negative burr formation with modified tool (MT) geometry

Figure 2c, represents the 3D chip morphology with MT geometry. Initially, the central section of convex shaped tool (at Z = 0) comes in contact with the workpiece material and onwards gradually contact between tool rake face and workpiece is built to the remaining width of workpiece (from Z = 0 towards Z = ±2). This promotes the lateral flow of material towards workpiece edges. Therefore, slight segmentation is visible on 3D chip near chip edges (Z = +2 and -2). While chip morphology is continuous around middle section (Z = 0). Figure 3c and 3d represent the location of pivot point and negative shear zone at the middle section (Z = 0). Pivot point is shifted towards workpiece free surface and negative shear zone is thin, in comparison with that produced with original insert (Fig. 3a and 3b). Figure 4b quantifies workpiece edge fracture and negative burr formation. Fig. 5c and 5d represent chip formation at sections Z = ±1.5 and ±2, respectively at the same cutting time. Comparison of Fig. 4b and 5c and 5d shows that at the same cutting time negative burr has been formed in middle section (Z = 0, Fig. 4b), while workpiece material is still in contact at the sections near workpiece edges (at Z = ±1.5 and ±2). This non-uniform tool-workpiece contact condition along width of cut, a_P restricts the tearing of material and early escape of uncut material from cutting and chip formation process. This decreases the generation of the negative burr formation as can be figured out in Fig. 4b.

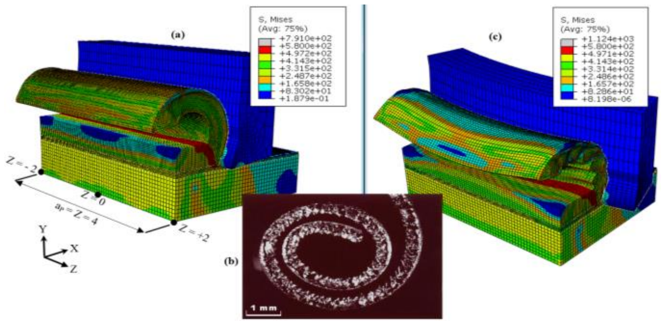

Fig. 2 3D Chip (a) Simulated with original tool (b) Experimental (c) Simulated with modified tool geometry

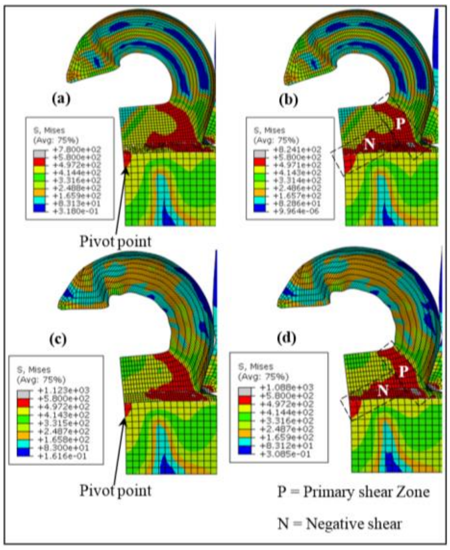

Fig. 3 Chip morphology at Z = 0 (a) Location of pivot point for original tool (b) Negative shear zone for original tool (c) Location of pivot point for modified tool geometry (d) Negative shear zone for modified tool geometry

May – June 2020
ISSN: 0193-4120 Page No. 1163 - 1167

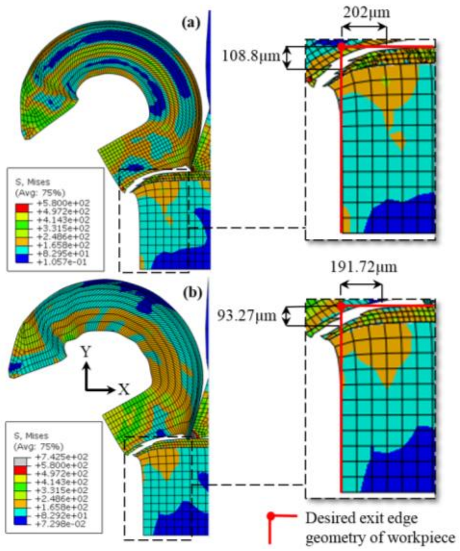

Fig. 4 Edge breakout (Negative burr) and boot type chip morphology at Z = 0 (a) with original tool (b) with modified tool geometry

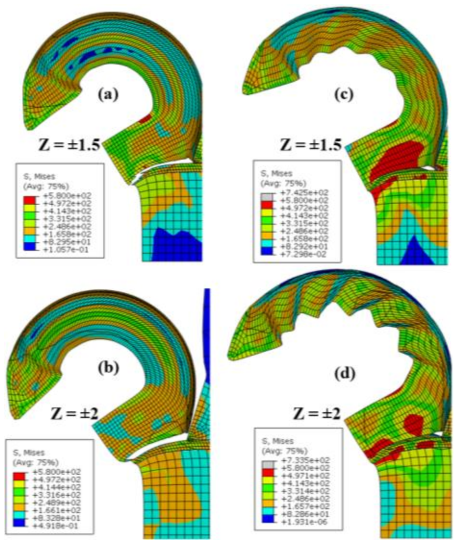

Fig. 5 Edge breakout (Negative burr) and boot type chip morphology (a) with original tool at Z = ±1.5 (b) with original tool at Z = ±2 (c) with modified tool geometry at Z = ±1.5 (d) with modified tool geometry at Z = ±2

IV. CONCLUSIONS

FE based numerical approach to simulate 3D chip and negative burr formation for turning aluminium alloy AA2024-T351 has been presented in this contribution. At workpiece exit edge negative shear zone is generated below workpiece free surface due to excessive bending loads. A crack/fracture in the workpiece in front of tool tip initiates and material escapes from cutting action leading to boot type chip formation. Some material at the exit edge breaks and taken away by the chip. This edge breakout is termed as negative burr. A modified convex shaped tool has been proposed. This tool geometry produces non-uniform contact condition at tool-workpiece interface along width of cut. This restricts the uniform tearing of material at workpiece edge along width of cut and material passes through the actual cutting and chip formation process, leading to decrease in negative burr.

ACKNOWLEDGMENT

Technical discussions on scope of paper, and numerical simulation with Pr. Dr. Tarek Mabrouki, ENIT, Tunis are highly acknowledged.

REFERENCES

[1] S. A. Niknam, B. Davoodi, J. P. Davim, S. Victor, “Mechanical deburring and edge-finishing processes for aluminum parts—a review”, *Int. J. Adv. Manuf. Technol.* 2018, 95, pp.1101-1125.

[2] J. C. Aurich, D. A. Dornfeld, P. J. Arrazola, V. Franke, L. Leitz, S. Min, “Burrs—Analysis, control and removal”, *CIRP Annals – Manuf. Tech.* 2009, 58, pp. 519–542.

[3] M. Asad, H. Ijaz, M. A. Khan, T. Mabrouki, W. Saleem, “Turning modeling and simulation of an aerospace grade aluminum alloy using two-dimensional and three-dimensional finite element method”, *Proc. Inst. Mech. Eng., B J. Eng. Manuf.* 2014, 228, pp.367–375.

[4] M. Asad, H. Ijaz, W. Saleem, A. S. B. Mahfouz, Z. Ahmad, T. Mabrouki, “Finite Element Analysis and Statistical Optimization of End-Burr in Turning AA2024”, *Metals* 2019, 9, pp.276.

[5] C. H. Chu, D. A. Dornfeld, “Tool path planning for avoiding exit burrs” *J. Manuf. Process.* 2000, 2, pp.116–123.

[6] R. Narayanaswami, D. A. Dornfeld, “Burr Minimization in Face Milling: A Geometric Approach”, *J. Manuf. Sci. Eng.* 1997, 119, pp. 170–177.

[7] M. Asad, “Elaboration of concepts and methodologies to study peripheral down-cut milling process from macro-to-micro scales” *PhD thesis, INSA of Lyon, 2010, France*

[8] H. Ijaz, M. Zain-ul-abdein, et al., “Modified johnson-cook plasticity model with damage evolution: application to turning simulation of 2xxx aluminium alloy”, *J. Mechanics* 2017, 33, pp. 777–788.

[9] H Ijaz, M Zain-ul-abdein et al., “Numerical simulation of the effects of elastic anisotropy and grain size upon the machining of AA2024”, *Mach. Sci.Technol.* 2018, 22, pp.522-542.
[10] W Saleem, M Zain-ul-abdein et al., “Computational Analysis and Artificial Neural Network Optimization of Dry Turning Parameters—AA2024-T351”, *App. Sci.* 2017, 7, pp. 642.
[11] S. Subbiah, S. N. Melkote, “Effect of finite edge radius on ductile fracture ahead of the cutting tool edge in 633 micro-cutting of Al2024-T3”, *Materials Science and Engineering A* 2008 474, pp. 283–300.
[12] A. Hillerborg, M. Modéer, P. E. Petersson, “Analysis of crack formation and crack growth in concrete by means of fracture mechanics and finite elements”, *Cem. Concr. Res.* 1976, 6, pp. 773–782.

Abbreviations and Acronyms

A	Initial yield stress (MPa)
a_P	Cutting depth or axial depth of cut (mm)
B	Hardening modulus (MPa)
C	Strain rate dependency coefficient
C_p	Specific heat ($Jkg^{-1}°C^{-1}$)
D	damage evolution parameter
$D_1 \ldots D_5$	Coefficients of Johnson-Cook material shear failure initiation criterion
E	Young’s modulus (MPa)
f	Feed rate (mm/rev)
G_f	Fracture energy (N/m)
$K_{C\,I,\,II}$	Fracture toughness ($\mathrm{MPa}\sqrt{\mathrm{m}}$) for failure mode *I* and mode *II*
m	Thermal softening coefficient
n	Work-hardening exponent
P	Hydrostatic pressure (MPa)
T	Temperature at a given instant (°C)
T_m	Melting temperature (°C)
T_r	Room temperature (°C)
$\bar{u}$	Equivalent plastic displacement (mm)
$\bar{u}_f$	Equivalent plastic displacement at failure
Δu	Relative displacement of element (mm)
V_C	Cutting speed (m/min)
$P/\bar{\sigma}$	Stress triaxiality
$\bar{\varepsilon}$	Equivalent plastic strain
$\dot{\bar{\varepsilon}}$	Plastic strain rate (s^{-1})
$\dot{\bar{\varepsilon}}_0$	Reference strain rate (10^{-3} s^{-1})
$\bar{\varepsilon}_f$	Equivalent plastic strain at failure
$\Delta\bar{\varepsilon}$	Equivalent plastic strain increment
$\bar{\varepsilon}_{0i}$	Plastic strain at damage initiation
σ_{JC}	Johnson-Cook equivalent stress (MPa)
σ_y	Yield stress (MPa)
ω	Damage initiation criterion
ν	Poisson's ratio
α_d	Expansion coefficient ($\mu m.m^{-1}°C^{-1}$)
λ	Thermal conductivity ($W\ m^{-1}C^{-1}$)
λ_s	Mill helix angle (deg)
ρ	Density (kg/m^3)

AUTHORS PROFILE

Muhammad Asad is working as ~~an~~ Assistant Professor in College of Engineering, Prince Mohammad Bin Fahd University (PMU), Saudi Arabia. Modeling & simulation of manufacturing processes are the areas of his research interest since 2006. He also keeps more than 10 years of industrial experience in manufacturing and design industries.